Supporting Information

Axial Sulfur Ligand-Induced Coordination Symmetry Breaking in Co–N_4 Motifs for Enhanced Oxygen Reduction Reaction and Durable Rechargeable Zinc-Air Batteries

Zhen Meng[a,b†], Tingting Ma[a,b†], Jinxin Li[a,b], Kaijiong Guo[a,b], Jiangdu Huang[a,b], Shasha Tian[a,b], Yuen Qin[a,b], Dayong Fan[a,b], Huidan Lu[a,b]*, Yongping Liu[a,b]*, and Sundaram Chandrasekaran[a,b]*

[a]Guangxi Key Laboratory of Electrochemical and Magneto-chemical, Functional Materials, College of Chemistry and Bioengineering, Guilin University of Technology, Guilin 541004, PR China
[b]Guangxi Colleges and Universities Key Laboratory of surface and interface electrochemistry, College of Chemistry and Bioengineering, Guilin University of Technology, Guilin 541004, PR China

[†]- These authors contributed equally

Email:
Yongping Liu: liuyp624@163.com
Huidan Lu: lhuidangl@163.com
Sundaram Chandrasekaran: yes.chandrasekaran@gmail.com & chandru@glut.edu.cn

1. Experimental section

1.1 Materials and Methods

1.1.1 Chemical reagents

Cobalt (II) chloride hexahydrate ($CoCl_2 \cdot 6H_2O$) was attained from Aladdin Biochemical Technology Co., Ltd. (P. R. China). γ-cyclodextrin (γ-CD; $C_{48}H_{80}O_{40}$) was purchased from Ron Reagents (P. R. China). Sublimed sulfur was sourced from Cologne Chemicals, (P. R. China). Dicyandiamide ($C_2H_4N_4$) was acquired from Macklin Reagents, (P. R. China). Methanol (anhydrous) was supplied by Fuyu Fine Chemical Co., Ltd. (P. R. China). Solution of Nafion (5 wt%) was obtained from DuPont D520/DE520. (USA). The 20 wt.% commercial Pt/C obtained from Science Materials Station (P. R. China).

1.2 Preparation of NC and S–N–C catalysts

1.2.1 Synthesis of CD–MOF precursor: Initially, γ-cyclodextrin (γ-CD, 750 mg) was dissolved in methanol (50 mL) with stirring for 30 min at room temperature. The mixture was kept in the dark and allowed to stand undisturbed for 24 h. After the reaction, the product was collected by centrifugation. After being washed three times with ethanol, the product was dried at 60 °C, yielding a fine powder denoted as CD–MOF.

1.2.2. Synthesis of NC catalyst: The CD–MOF precursor (200 mg) was thoroughly mixed with dicyandiamide (200 mg, 1:1 mass ratio) as N source. Calcination was carried out in a tubular furnace under a N_2 flow (50 sccm) by heating the sample to 1000 °C at 5 °C min^{-1} followed by a 2 h hold. This process yielded the NC catalyst.

1.2.3 Synthesis of S–N–C Catalyst: The CD-MOF precursor (200 mg) was mixed with dicyandiamide (200 mg) and sublimed sulfur (300 mg, 1:1.5 mass ratio for CD–MOF/S) as N and S sources, respectively. Employing the identical calcination protocol established for the N–C catalyst, the mixture in an alumina boat was heated to produce the S–N–C material.

1.3 Preparation of Co–C, Co–N–C, and S–Co–N–C catalysts

1.3.1 Synthesis of Co–CD–MOF precursor: Initially, γ-cyclodextrin (750 mg) was dissolved in anhydrous methanol (50 mL) under stirring. Subsequently, cobalt(II) chloride hexahydrate (238 mg) was introduced into the solution, and stirring was continued for 30 min. The mixture was kept in the dark and allowed to stand undisturbed for 24 h. After being

washed three times with ethanol, the product was dried at 60 °C to get a fine powder, labeled as Co–CD–MOF.

1.3.2 Synthesis of S–Co–N–C catalyst: The Co–CD–MOF precursor (200 mg) was mixed with sublimed sulfur (300 mg) and dicyandiamide (200 mg), the mass ratio of 1:1.5 of S and N sources, respectively. Calcination was carried out in a tubular furnace under a N_2 flow (50 sccm) by heating the sample to 1000 °C at 5 °C min^{-1} followed by a 2 h hold. This process yielded the CoSACs-SNC/Co@C, and hereafter referred to as S–Co–N–C.

1.3.3 Synthesis of control samples: For comparative studies, control catalysts were synthesized under identical conditions. (i) Co–C was prepared using Co–CD–MOF without additional S and N sources under identical conditions to those used for the NC catalyst, (ii) Co–N–C was prepared using Co–CD–MOF with dicyandiamide (200 mg) without S, and (iii) S–Co–C was prepared using Co–CD–MOF with sublimed sulfur (300 mg) without dicyandiamide, otherwise under identical conditions to those used for the S–Co–N–C. To further investigate the influence of the sulfurization process, catalysts with Co–CD–MOF to S/N mass ratios of 1:1, and 1:2 were prepared, yielding S(1)–Co–N–C, and S(2)–Co–N–C, respectively. Whereas, the all other identical conditions were similar to those used for the S–Co–N–C. Besides, to study the temperature effect, calcination was performed for CoSACs-SNC/Co@C (labeled as S–Co–N–C) at 800 °C and 900 °C, producing S–Co–N–C-800 and S–Co–N–C-900.

1.4 Characterizations

The scanning electron microscopy (SEM) images and energy dispersive spectroscopy (EDS) were obtained by using Hitachi SU5000 field emission scanning electron microscopy and energy dispersive spectrometer at a working voltage of 5 kV. Transmission electron microscopy (TEM) imaging and energy dispersive X-ray spectroscopy (EDS) were performed under FEI TALOS-F 200X mode field emission transmission electron microscope and energy chromatograph at an accelerated voltage of 200 kV. High-angular dark-field scanning transmission electron microscopy (HAADF-STEM) images were obtained by using a Titan Themsis Z microscope equipped with a probe spherical aberration corrector operating at 300kV. X-ray diffraction (XRD) profiles Cu Kα (λ = 1.5406 Å) radiation was collected on an

X'Pert3Powder multifunctional X-ray diffractometer. Quantitative analysis of trace metals was performed using an Agilent 7700 inductively coupled plasma mass spectrometry (ICP-MS) system. Raman spectroscopy was performed with a 532 nm Ar ion laser beam on the LabRAM HR Evolution confocal Micro-Raman spectrometer. X-ray photoelectron spectroscopy (XPS) was performed using a monochromatic Al-Kα X-ray source using a Thermo Scientific K-Alpha X-ray photoelectron spectrometer. The pore structure and specific surface area of the catalyst were analyzed by nitrogen (N_2) adsorption-desorption isotherm (Micromeritics ASAP 246).

X-ray absorption fine structure spectra (XAFS) have been obtained at the BL14W beamline station at the Shanghai Synchrotron Radiation Facility (SSRF) in China. While, Co foil, Co_2O_3, CoS_2, and cobalt phthalocyanine (CoPc) were used as references. Athena and Artemis in the IFEFFIT package are used to process the EXAFS data collected according to standard procedures. The obtained XAFS data was processed in Athena (version 0.9.26) for background, front edge line, and back edge line calibration.[1, 2] Fourier transform fitting was then performed in Artemis (version 0.9.26). Sample fitting was weighted by k^3, with k ranging from 3-11 Å cm^{-1} and R ranging from 1-4 Å cm^{-2}. The four parameters of coordination number (N), bond length (R), Debye-Waller factor, and E_0 displacement (ΔE_0) are fitted, and σ^2 is determined. For wavelet transform analysis, χ (k) derived from Athena was imported into the Hama Fortran code. The parameters are shown as follows: the *R* range of the sample is 0-6 Å λ, and the *k* range is 0-12 Å λ^{-1}; the weight of *k* is 3; the Morlet function of κ=10, σ=1 was used as the parent wavelet to provide the overall distribution.

1.5 Electrochemical Measurements

1.5.1 Preparation of working electrode

Prior to the fabrication of the working electrode, the catalyst was thoroughly grounded to ensure homogeneity. Subsequently, 2.5 mg of catalyst powder is weighed and combined with 25 μL of 5% Nafion solution and 475 μL of anhydrous ethanol. The mixture was subjected to ultrasonication for 30 min to obtain a uniform catalyst ink. A small amount of alumina (Al_2O_3) polishing powder was applied to wet chamois leather and the glassy carbon electrode (GCE) is polished using a figure-eight motion until a smooth and flat surface was achieved. After

rigorous rinsing and drying, 8 μL of the catalyst ink was drop-casted onto the surface of the glassy carbon electrode (diameter: 4 mm), followed by drying at ambient temperature to form a uniform catalyst film. The catalyst loading was controlled at 0.2 mg cm^{-2}. Subsequently, electrochemical measurements are carried out in 0.1 M KOH electrolytes using the modified electrode. For comparison, the mass loading of commercial 20 wt.% Pt/C is approximately 0.12 mg cm^{-2}.

1.5.2 Electrochemical performance test

All electrochemical measurements in this study were performed on a CHI760E electrochemical workstation, a standard three-electrode system was used for testing, with platinum (Pt) wire as the counter electrode, Hg/HgO electrode as the reference electrode, and glassy carbon electrode (GCE) loaded with catalyst ink as the working electrode. All experiments were carried out at an ambient temperature of 25°C using 0.1 M KOH as the electrolytes. Prior to each measurement, the electrolytes were purged with O_2 or N_2 gas for at least 30 min to achieve saturation. Based on the Nernst equation, all potentials recorded versus the Hg/HgO reference electrode were converted to the reversible hydrogen electrode (RHE) scale according to equation (1-1):

$$E(vs.RHE) = E(vs.Hg/HgO) + 0.098 + 0.0591 \times pH \qquad (1\text{-}1)$$

Cyclic voltammetry tests were conducted at a scan rate of 0.2 V/s in 0.1 M KOH electrolytes saturated with N_2 and O_2, respectively. The scan range was 0.3 V to -0.8 V, with 40 cycles performed to activate the catalyst. Simultaneously, the double-layer capacitance (C_{dl}) of the catalyst can be calculated by testing CV curves at different scan rates. Given the double-layer capacitance, the electrocatalytic active surface area (ECSA) can be estimated using equation (1-2):

$$ESCA = \frac{C_{dl}}{C_S} \qquad (1\text{-}2)$$

C_S is the specific capacitance of the catalyst, and in 0.1 M KOH solution, C_S takes a value ranging from 0.022 to 0.130 mF cm^{-2}, it is uniformly taken as 0.040 mF cm^{-2}.

Before testing the LSV, the electrolyte was also saturated with O_2 for more than half an hour, and IR drop compensation (90%) was used to eliminate the effect of solution resistance,

with a linear scanning range of 0.3 V to -0.8 V and a scanning rate of 0.01 V sec^{-1}. The rotational speed of the rotating disc electrodes was kept constant at 1600 rpm, and the electron transfer number (n) for ORR was calculated from the LSV at different speeds: 2400 rpm, 2000 rpm, 1600 rpm, 1200 rpm, 800 rpm, and 400 rpm by using the *K-L* (Koutecky-Levich) equation:

$$\frac{1}{J}=\frac{1}{J_L}+\frac{1}{J_K}=\frac{1}{B\omega^{\frac{1}{2}}}+\frac{1}{J_K} \quad (1\text{-}3)$$

$$B=0.2nFC_{o_2}\left(D_{o_2}\right)^{\frac{2}{3}}v^{-\frac{1}{6}} \quad (1\text{-}4)$$

J is the current measured in the experiment; J_L is the kinetic control current of the RDE; J_K is the diffusion limit current of the RDE; n is the number of electron transfers in the ORR; F is Faraday's constant, with a magnitude of 96485 C/mol; the concentration of C_{O2} oxygen, with a pH range of 5~13, is 1.2 × 10^{-3} mol cm^{-3}; D_{O2} is the diffusion rate of oxygen molecules, which is 1.9 × 10^{-5} cm^2 s^{-1} for the pH range of 5 to 13; ω is the rotational speed of the disc electrode (RDE) in rad s^{-1}; $0.2nFC_{o_2}\left(D_{o_2}\right)^{\frac{2}{3}}v^{-\frac{1}{6}}$ is denoted as K; and v is the kinetic viscosity of the solution, which is taken as the value of 0.01 cm^2 s^{-1}. From this, the plotting of the experimental data gives the number of electron transfers from the ORR.

The Tafel slopes are all measured at 1600 rpm LSV curves then converted as follows:

$$\eta=b\log\left(\frac{j}{j_0}\right)+a \quad (1\text{-}6)$$

η is the overpotential, a is the Tafel coefficient, b is the Tafel slope, j is the current density, and j_0 exchange current density.

The turnover frequency (TOF) for the oxygen reduction reaction (ORR) at 0.7 V *vs.* RHE was determined using the formula:[3, 4]

$$TOF=\frac{j_k N_e}{\omega c N_A/M} \quad (1\text{-}7)$$

where J_k represents the kinetic current density (A cm^{-2}), N_e is the electron number per

Coulomb (6.22×10^{18} C^{-1}), ω denotes the content of active metal (*wt*.%), *c* is the catalyst loading (g cm^{-2}), NA is the Avogadro constant (6.022×10^{23} mol^{-1}), and M is the molar mass of active metal (g mol^{-1}).

1.6. Preparation and assembly of rechargeable zinc-air batteries (ZABs)

To evaluate the overall catalytic performance, rechargeable zinc–air batteries were assembled using laboratory-made electrochemical cells. A polished zinc (Zn) plate (~0.2 mm thick) and a glass fiber diaphragm (average pore size ~1.63 μm, thickness ~0.29 mm) were purchased from Ouleji (Chongqing) Zinc Materials Co., Ltd., China. The composite electrode matrix, consisting of nickel foam, a hydrophobic permeable membrane, and carbon paper arranged from bottom to top, was obtained from Changsha Spring N_2 Company, China. The catalyst was used as an air cathode on an electrode composite substrate (nickel foam, hydrophobic breathable film, and carbon paper stacked densely from bottom to top in sequence). A polished zinc (Zn) plate was used as the anode and a mixture of 6 M KOH with 0.2 M Zn $(CH_3CO_2)_2$ were used as the electrolytes. The battery unit is assembled sequentially from the air positive electrode and the Zn plate negative electrode, and the circulation pump unit was connected to the inlet and outlet on the outside of the battery mould. Finally, a homemade rechargeable ZAB device with circulating electrolytes was formed by setting the circulation flow rate of the circulation pump to 10 mL min^{-1}. The electrode preparation was as follows, initially 9 mg of catalyst, 3mg of carbon black and 9 mg of polytetrafluoroethylene (PTFE) powder were weighed and mixed in 1.5 mL of ethanol in the ratio of 3:1:3, and ultrasonication was carried out for 60 min in order to form a uniformly dispersed ink. Further, certain size of the electrode composite substrate was cutted. Then a pipette gun was used to draw 500 μL of catalyst ink, and dropped it onto the surface of the electrode composite substrate in batches. The drop area was 3 cm^2 and the reaction area of the Zn air cell was 1 cm^2 to ensure a catalyst loading of 1 mg cm^{-2}. After the drop was completed, the electrodes were dried at room temperature for testing. In addition, another ZAB air cell was also assembled using commercial Pt/C and IrO_2 catalysts as air electrodes for comparison. The specific capacities of ZABs were tested using the chronopotential method. In this experiment, the ZABs was tested at a current density of 10 mA cm^{-2} using an electrochemical workstation

and the specific capacity of the battery was calculated based on the discharge time and zinc consumption. The formula for its calculation is as follows:

$$C = {(I \times t)}/{m_{z_n}} \quad (1\text{-}6)$$

whereas, C is the specific capacity of the ZABs ($mAhg^{-1}$), I is the discharge current (mA), t is the discharge time (h), and M_{Zn} is the mass of zinc plates consumed (g).

1.7. Density Functional Theory Calculations

All spin-polarized density functional theory (DFT) calculations were performed using the Quantum ESPRESSO package within the plane-wave pseudopotential framework[5-8]. The methodology was selected to balance accuracy with computational efficiency for surface and catalyst slab systems. The Co-N-C and S-Co-N-C structures were modeled as single transition metal atoms embedded in a graphene matrix, coordinated with four nitrogen atoms and/or one sulfur atom within a 5×5 orthogonal supercell. A vacuum layer of ~15 Å was included in the non-periodic direction to eliminate spurious interactions between periodic images. Geometry optimizations employed the Perdew-Burke-Ernzerhof (PBE) generalized gradient approximation (GGA) for the exchange-correlation functional[9, 10]. Core-valence electron interactions were treated using projector-augmented wave (PAW) pseudopotentials from the SSSP efficiency library, and van der Waals dispersion forces were incorporated using Grimme's DFT-D3 method[9, 10]. Kinetic energy cutoffs were determined via convergence testing. For the M-N-C catalyst models, a wavefunction cutoff of 50 Ry with a charge density cutoff of 200 Ry was found to be sufficient. A Marzari-Vanderbilt smearing of 0.01 Ry was applied. Given the large size and localized nature of the active site in these M-N-C models, Γ-point-only sampling was employed for the Brillouin zone, a standard and efficient practice for such isolated, low-dimensional systems. Structures were considered optimized when the force on each atom was less than 0.01 eV/Å. Electronic structure analysis, including projected density of states (PDOS) calculations, was performed on the fully relaxed geometries to elucidate bonding interactions and catalytic features. The Gibbs free energy of the reaction intermediates can be calculated by following previous reports.[5, 11, 12]

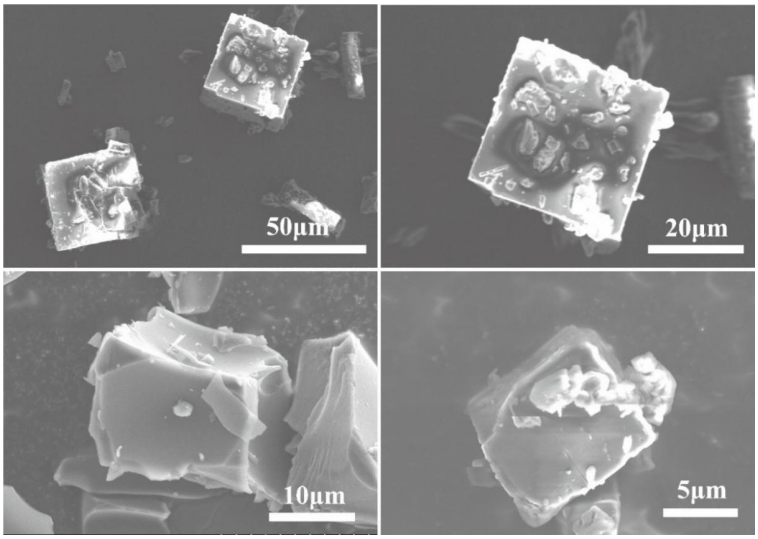

Fig. S1 SEM images of CD−MOF

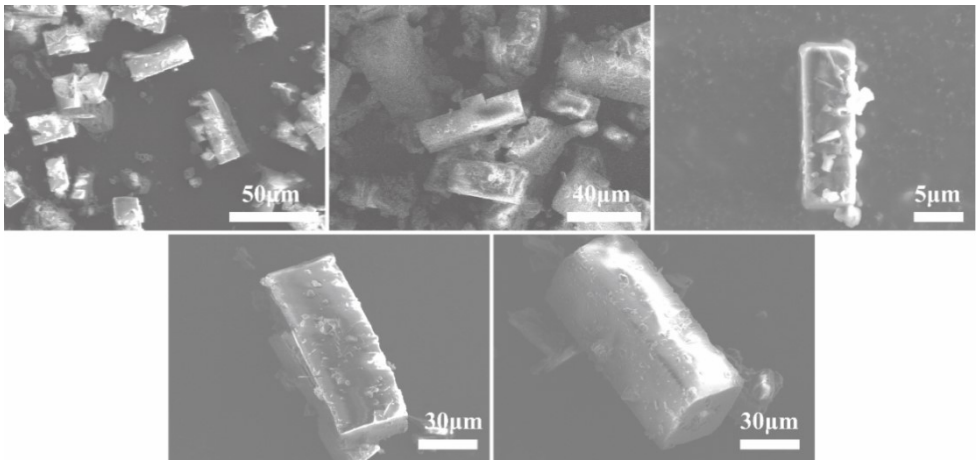

Fig. S2 SEM images of Co−CD−MOF

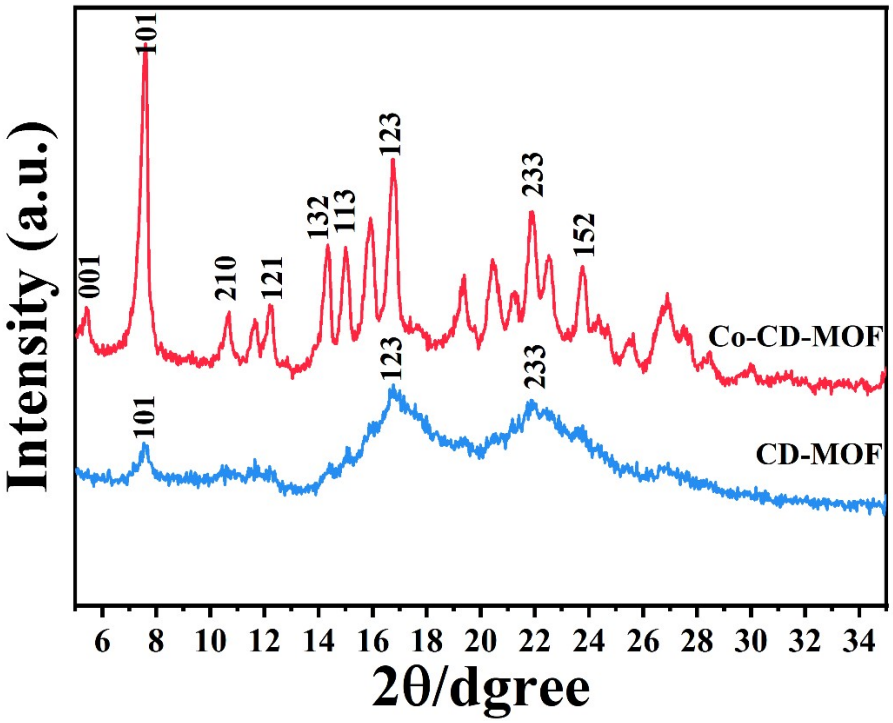

Fig. S3 XRD patterns of CD-MOF and Co-CD-MOF samples

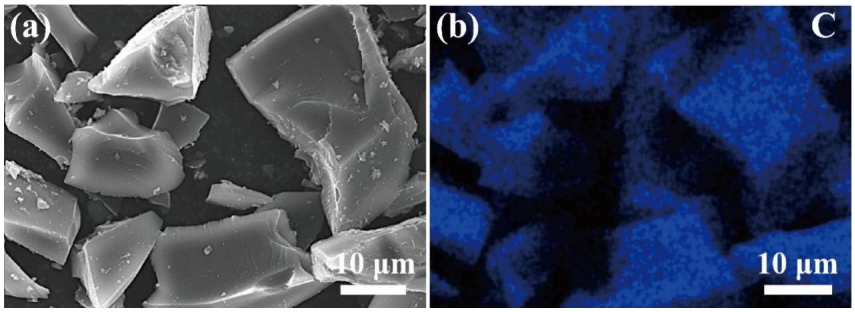

Fig. S4 SEM and EDS mapping of C catalyst

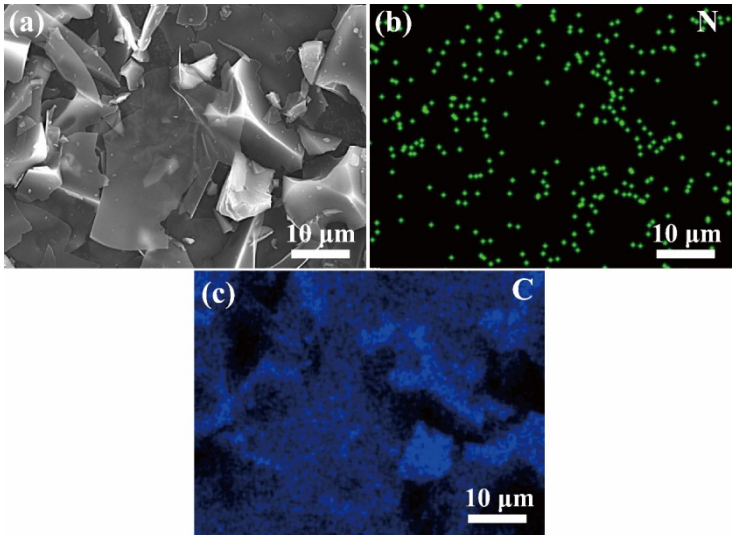

Fig. S5 SEM and EDS mapping of NC catalyst

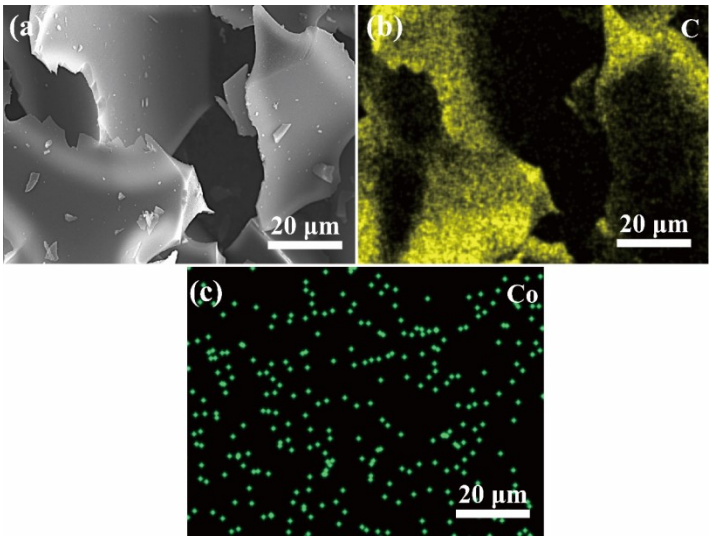

Fig. S6 SEM and EDS mapping of Co−C catalyst

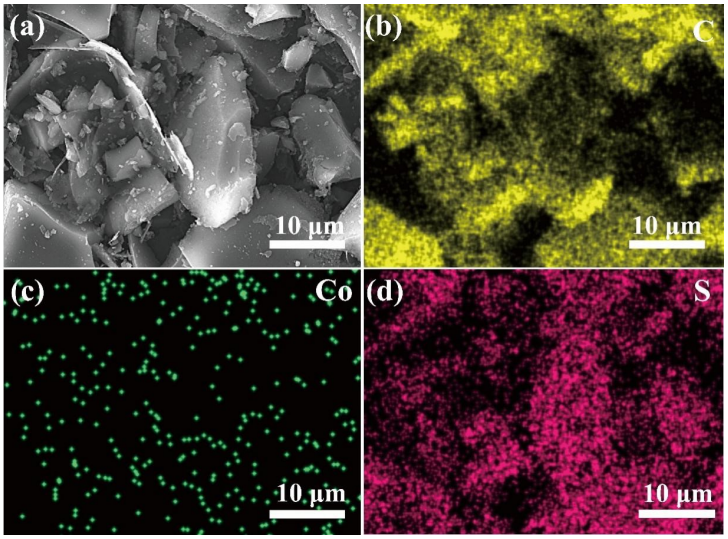

Fig. S7 SEM and EDS mapping of S−Co−C catalyst

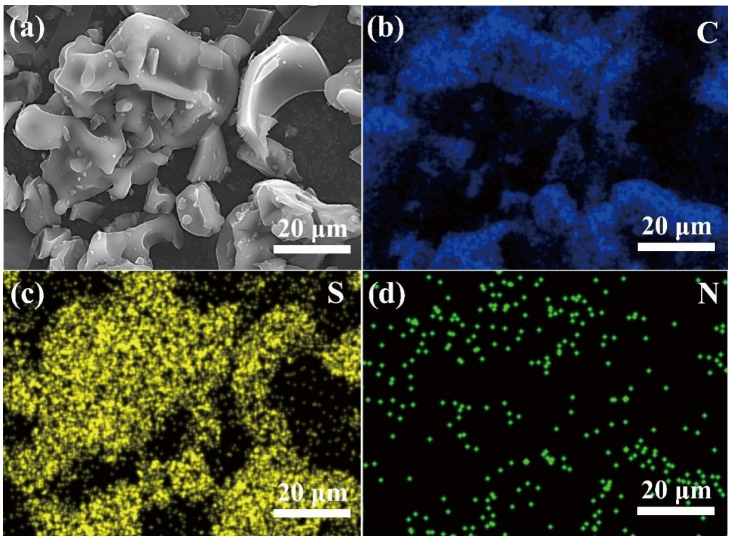

Fig. S8 SEM and EDS mapping of S−N−C catalyst

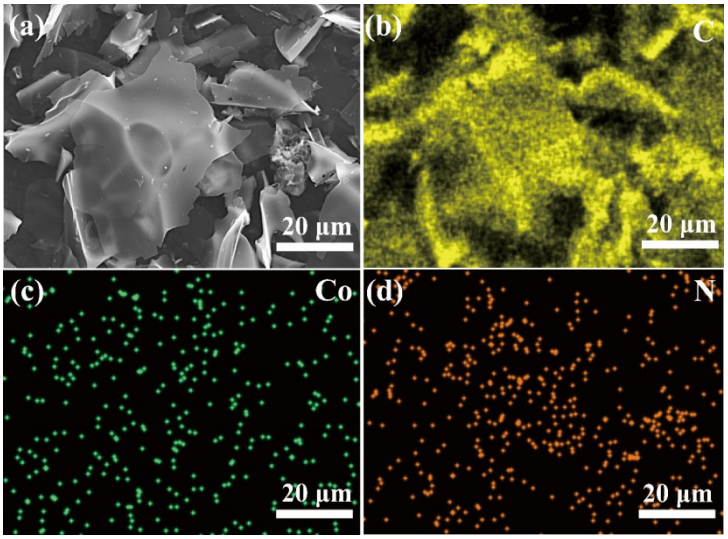

Fig. S9 SEM and EDS mapping of Co−N−C catalyst

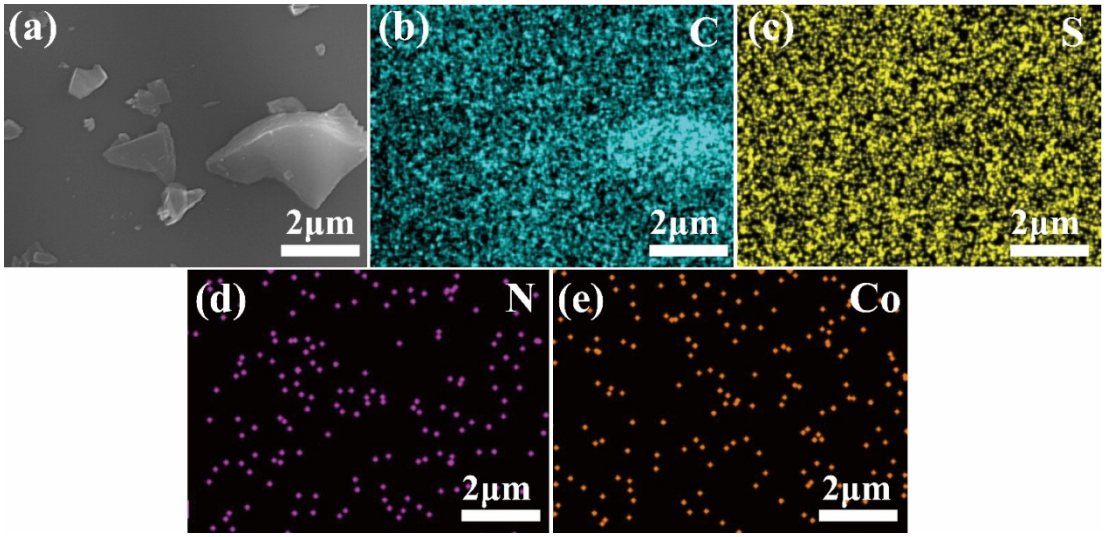

Fig. S10 SEM and EDS mapping of S(1)−Co−N−C catalyst

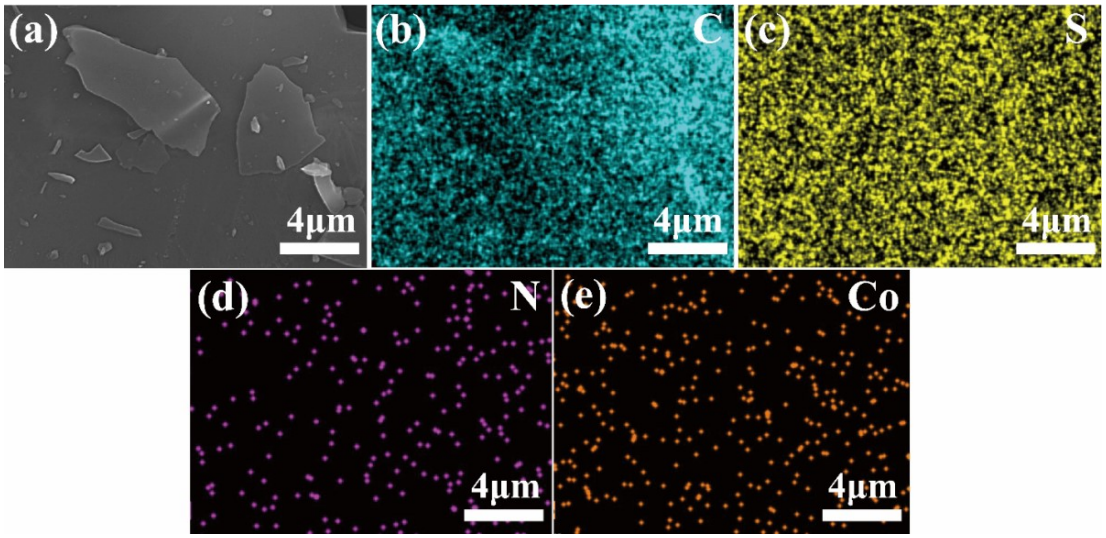

Fig. S11 SEM and EDS mapping of S(2)−Co−N−C catalyst

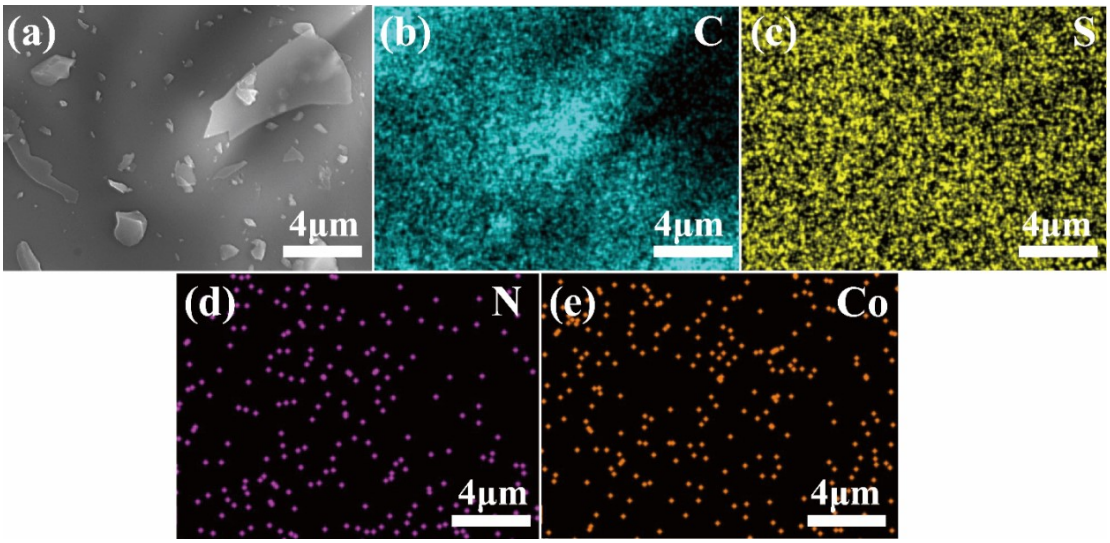

Fig. S12 SEM and EDS mapping of S−Co−N−C-800 catalyst

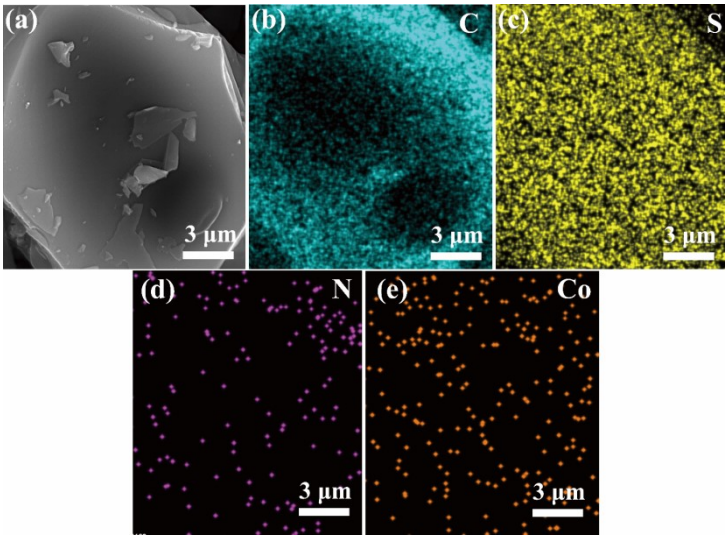

Fig. S13 SEM and EDS mapping of S−Co−N−C-900 catalyst

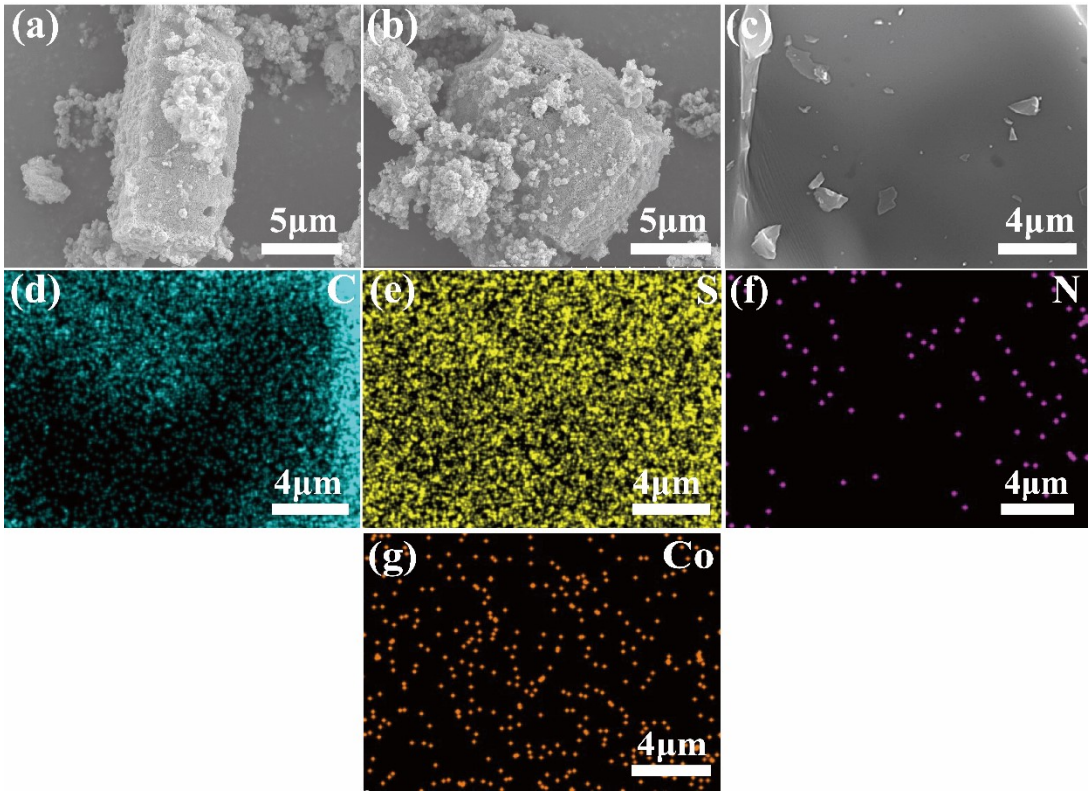

Fig. S14 SEM and EDS mapping of S−Co−N−C catalyst

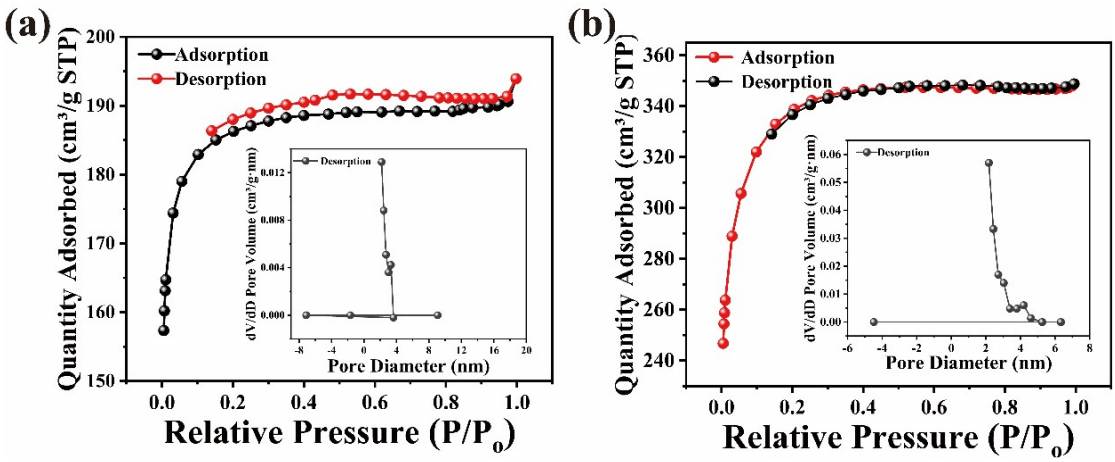

Fig. S15 N_2 adsorption-desorption isotherms and pore size distribution of (a) C and (b) S−Co−N−C catalysts, respectively.

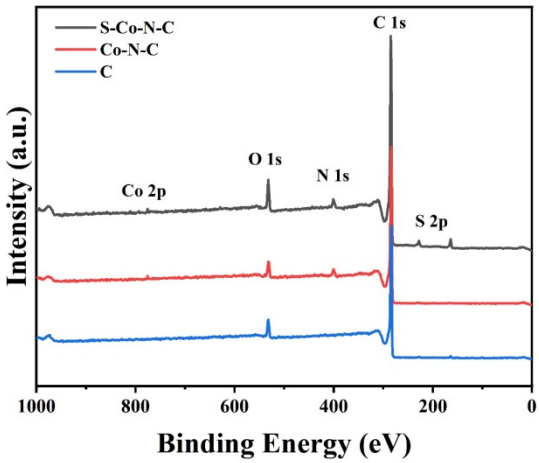

Fig. S16 XPS spectra of C, Co−N−C and S−Co−N−C catalysts

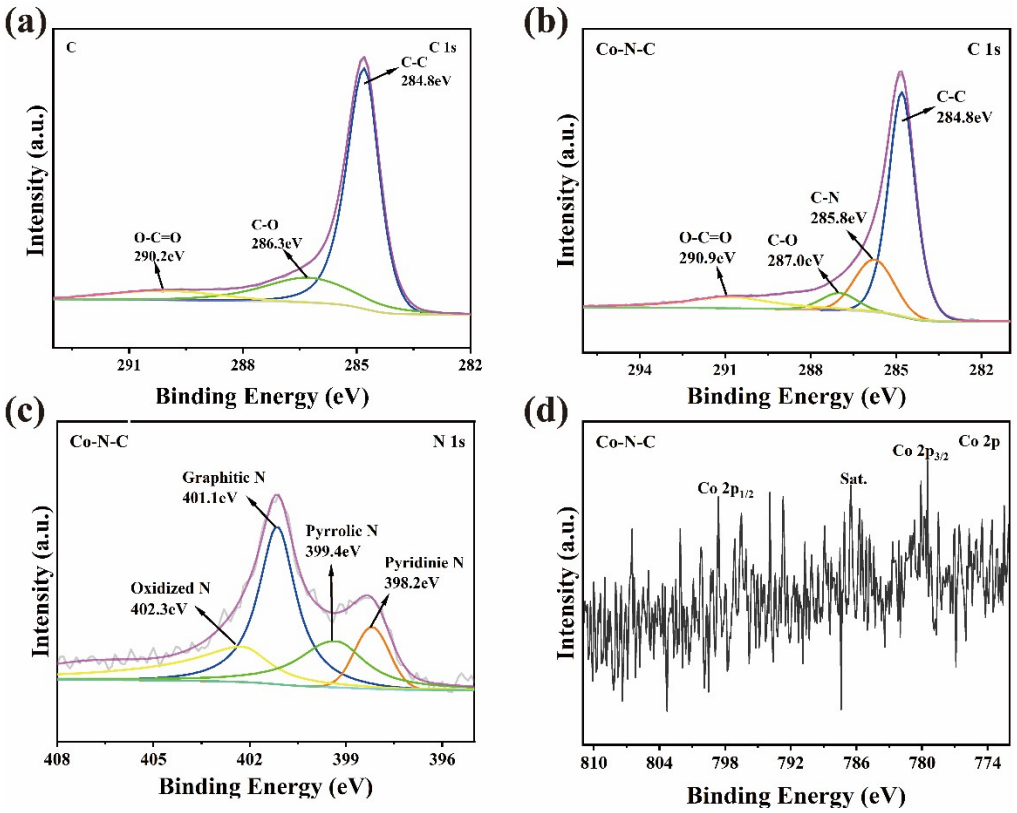

Fig. S17 XPS (a) C 1s core-level spectra of bare carbon catalyst and (b) C 1s and (c) N 1s and (d) Co 2p core-level spectra of Co−N−C catalyst

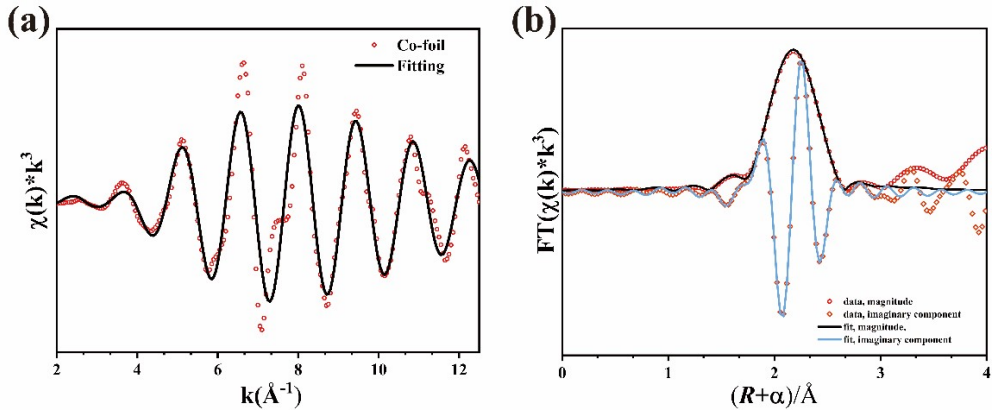

Fig. S18 EXAFS (a) k space fitting curves and (b) R space fitting curves of reference Co foils

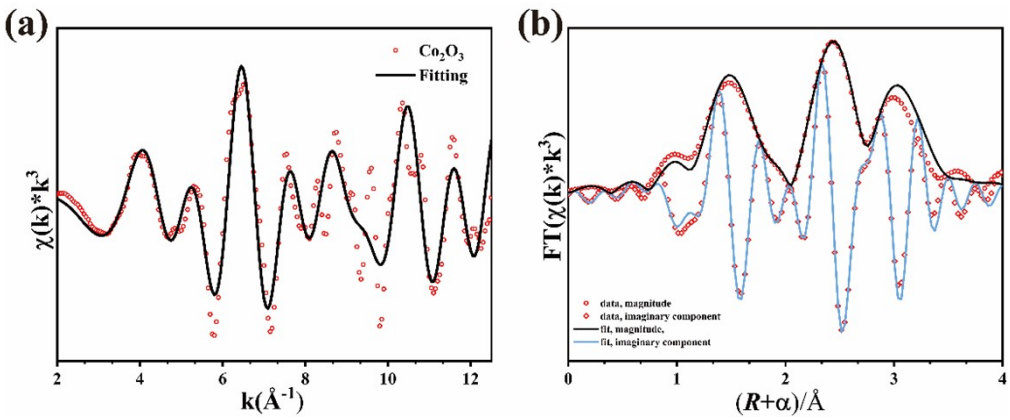

Fig. S19 EXAFS (a) k space fitting curves and (b) R space fitting curves of reference Co_2O_3

Table. S1 EXAFS fitting parameters at the Co K-edge for various samples (S_0^2=0.90)

Sample	Path	N[a]	R(Å)[b]	$\sigma^2(10^{-3}$ Å$^2)$[c]	R factor
Co-foil	Co-Co	3	2.49	5.53	0.00284
Co_2O_3	Co-Co1	4.85	3.38	5.10	0.00478
	Co-Co2	5.53	2.87	3.99	
	Co-O	3.73	1.92	1.27	
S−Co−N−C	Co-S	1.05	2.32	4.55	0.00478
	Co-N	3.96	2.00	8.72	
	Co-Co1	0.29	2.43	14.2	
	Co-Co2	2.04	3.00	3.55	

aN: coordination numbers; bR: bond distance; c crs; bR: bond distance; c cace fitting curves of re

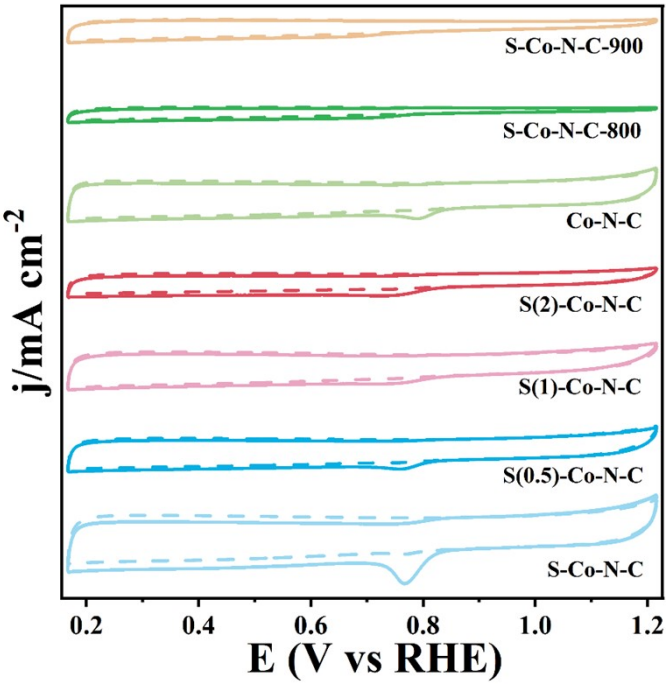

Fig. S20 CV profile of prepared catalysts in O_2 and N_2 saturated 0.1 M KOH electrolytes (solid line: O_2, dashed line: N_2)

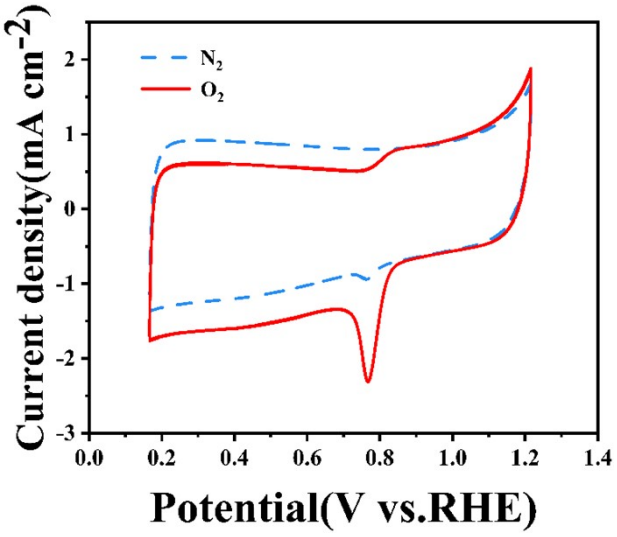

Fig. S21 CV profile of S−Co−N−C in O_2 and N_2 saturated 0.1 M KOH electrolytes (solid line: O_2, dashed line: N_2)

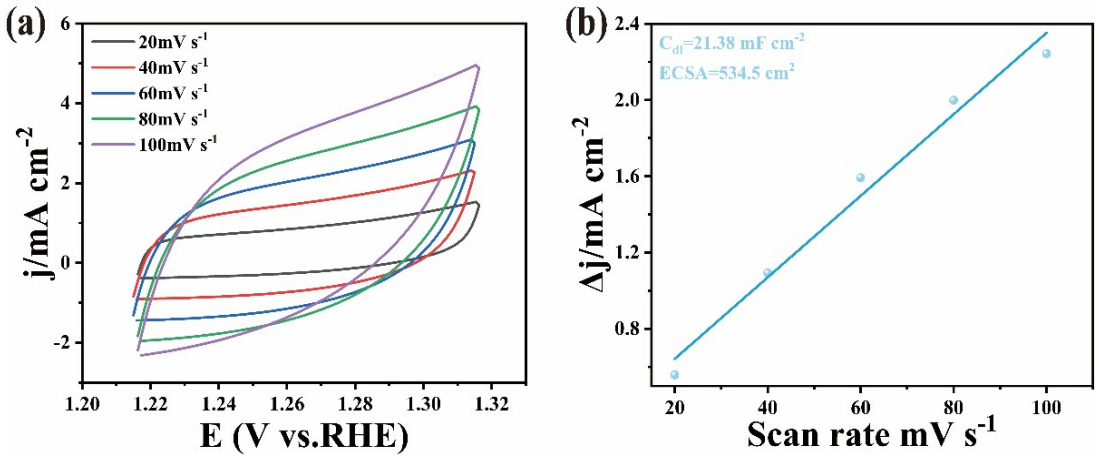

Fig. S22 (a-b) CV curves and their corresponding C_{dl} plots at different scan rates of S−Co−N−C, respectively.

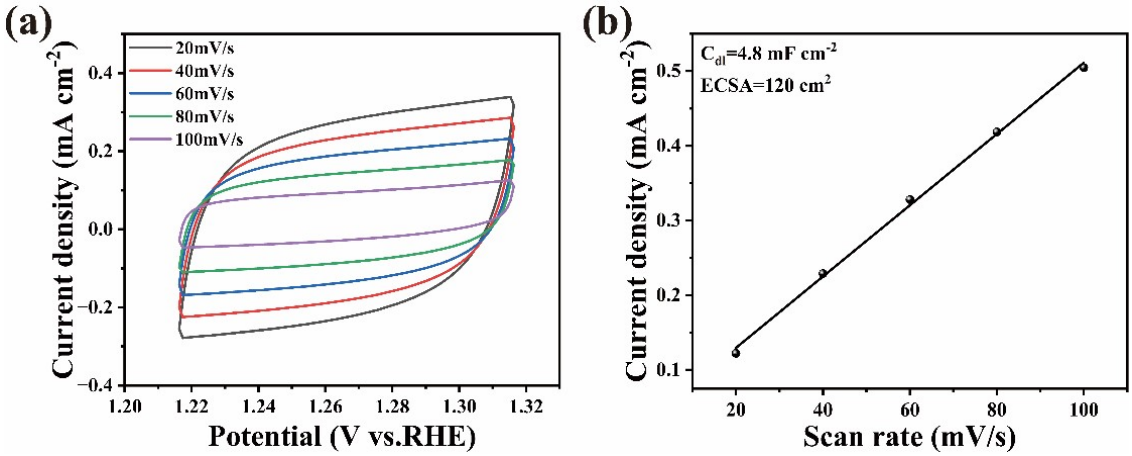

Fig. S23 (a-b) CV curves and their corresponding C_{dl} plots at different scan rates of C, respectively.

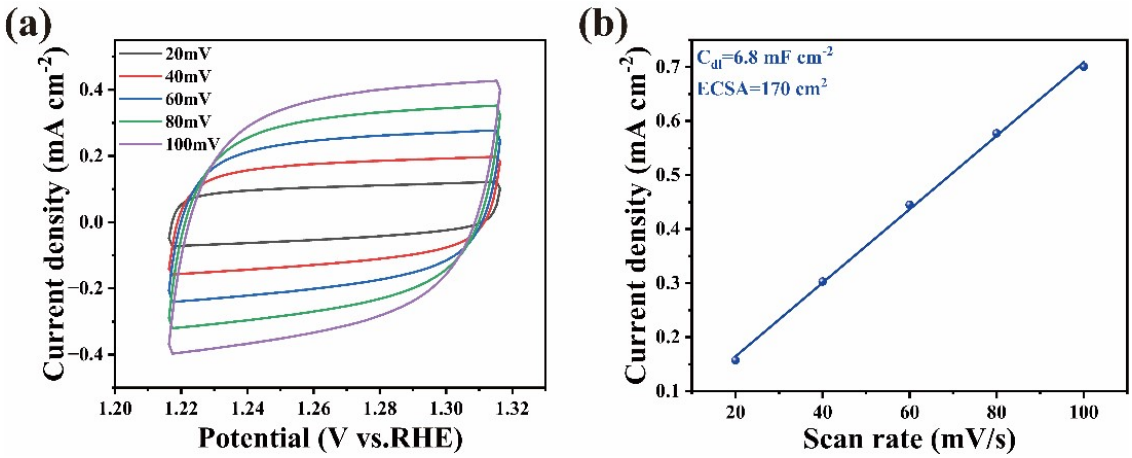

Fig. S24 (a-b) CV curves and their corresponding C_{dl} plots at different scan rates of NC, respectively.

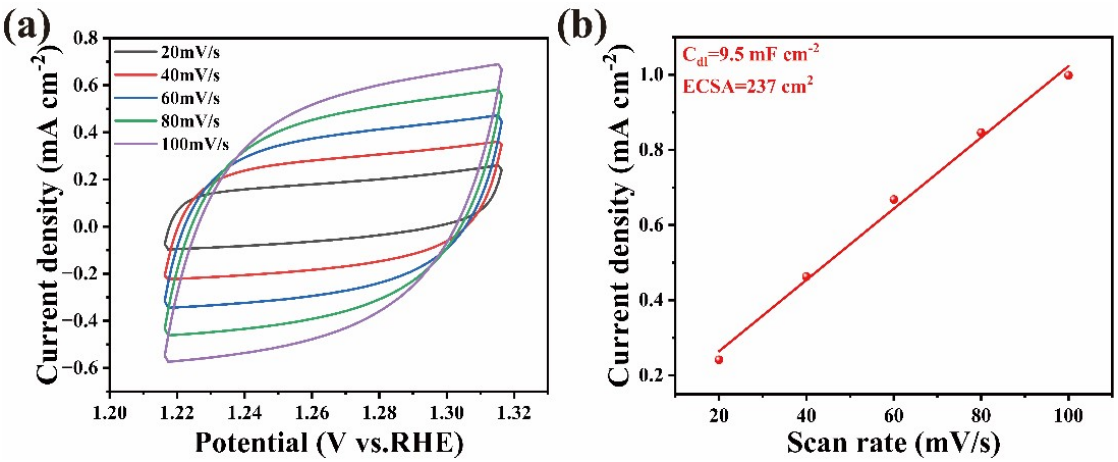

Fig. S25 (a-b) CV curves and their corresponding C_{dl} plots at different scan rates of Co−C, respectively.

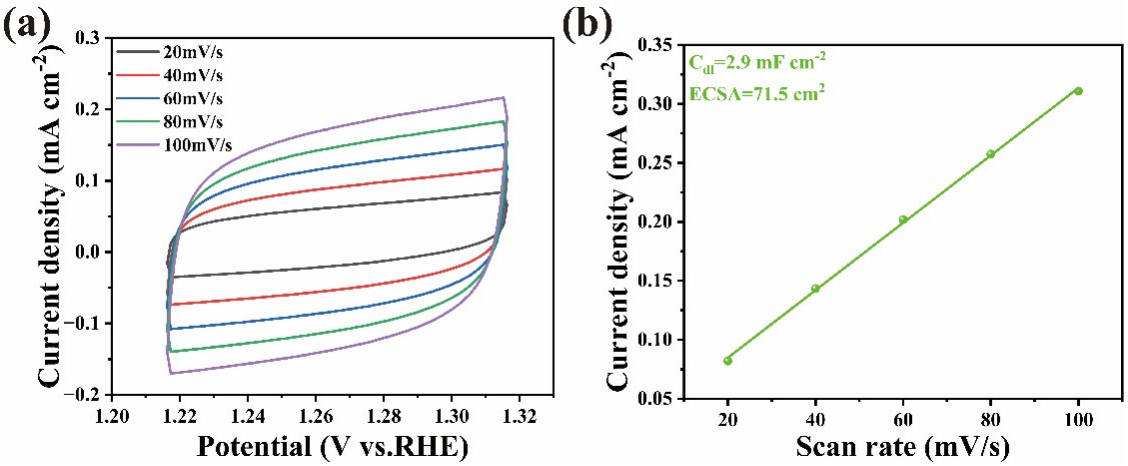

Fig. S26 (a-b) CV curves and their corresponding C_{dl} plots at different scan rates of Co−N−C, respectively.

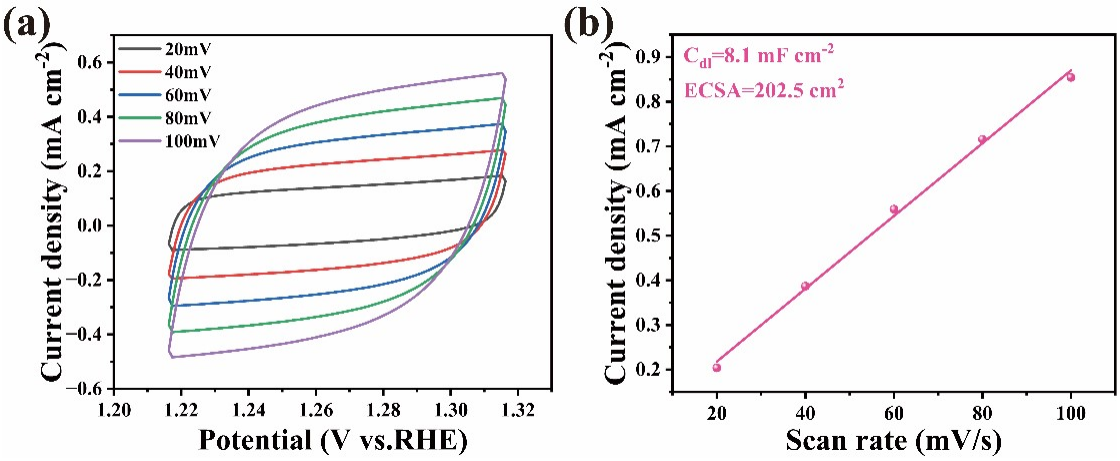

Fig. S27 (a-b) CV curves and their corresponding C_{dl} plots at different scan rates of S−N−C, respectively.

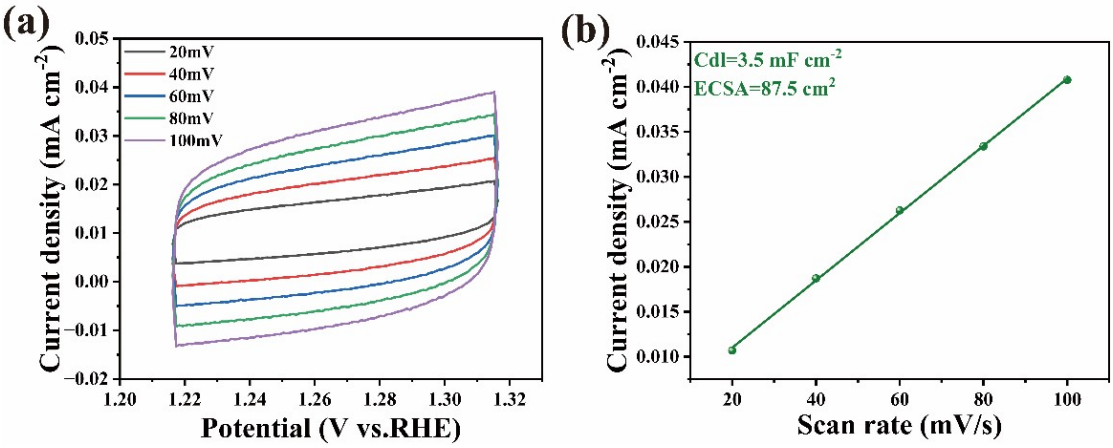

Fig. S28 (a-b) CV curves and their corresponding C_{dl} plots at different scan rates of S−Co−C, respectively.

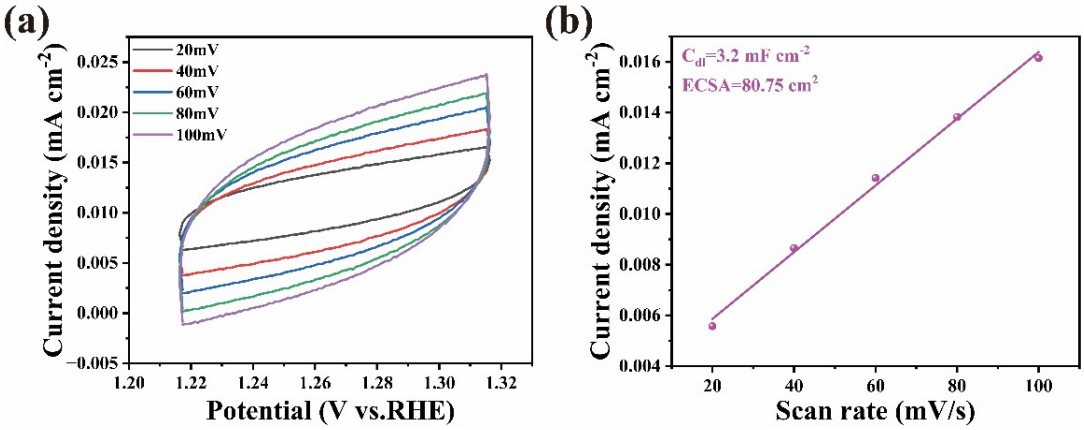

Fig. S29 (a-b) CV curves and their corresponding C_{dl} plots at different scan rates of S(1)−Co−N−C, respectively.

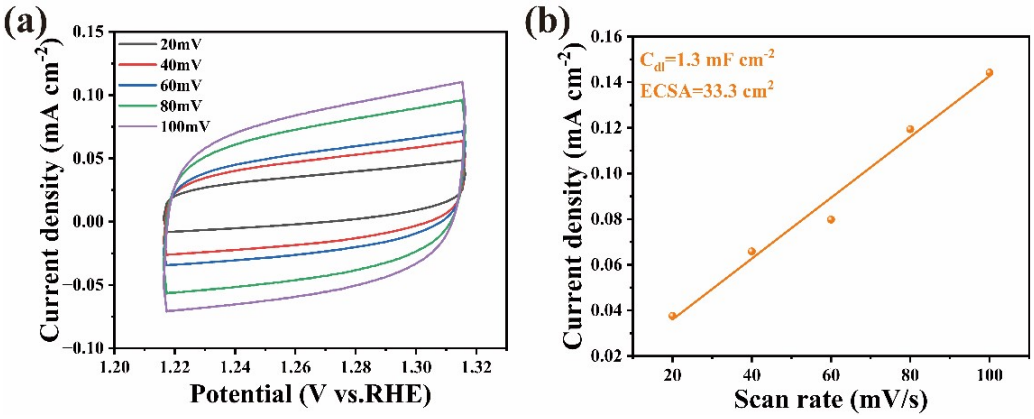

Fig. S30 (a-b) CV curves and their corresponding C_{dl} plots at different scan rates of S(2)−Co−N−C, respectively.

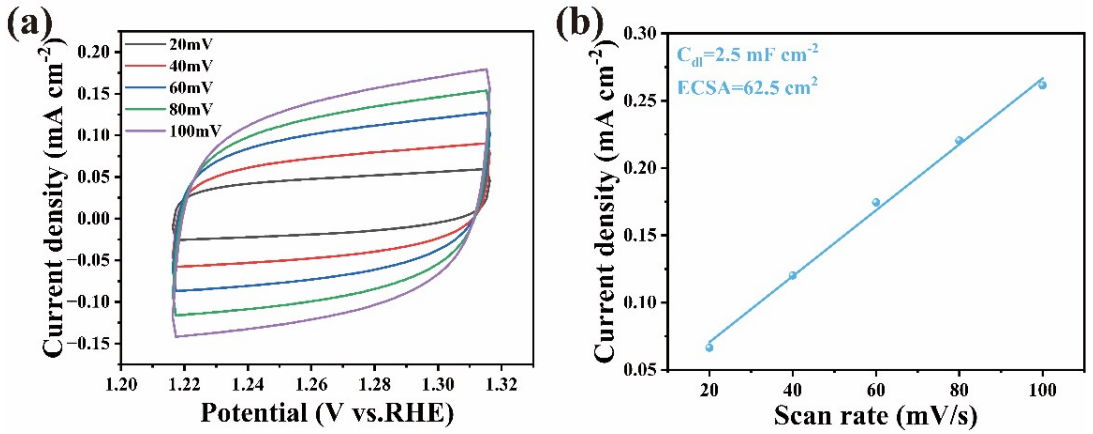

Fig. S31 (a-b) CV curves and their corresponding C_{dl} plots at different scan rates of S−Co−N−C-800, respectively.

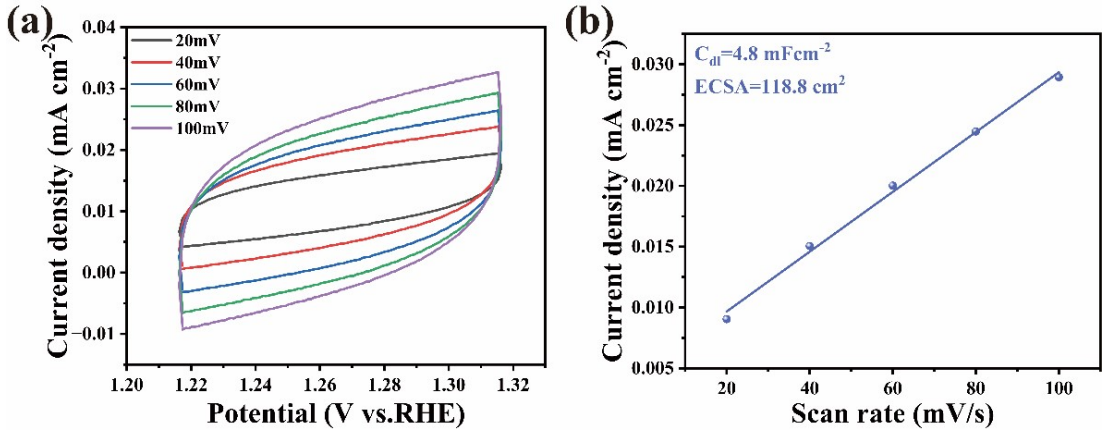

Fig. S32 (a-b) CV curves and their corresponding C_{dl} plots at different scan rates of S−Co−N−C-900, respectively.

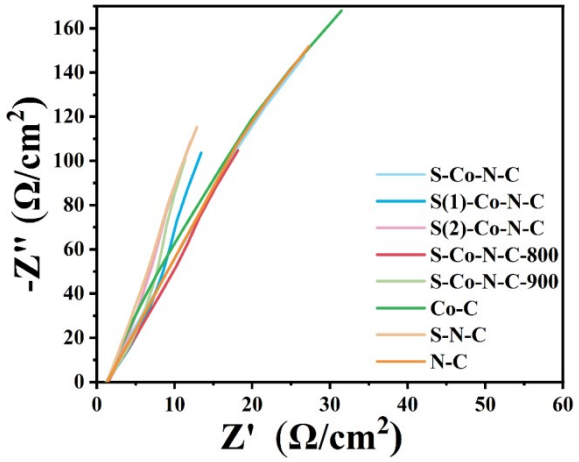

Fig. S33 EIS spectra for prepared catalysts

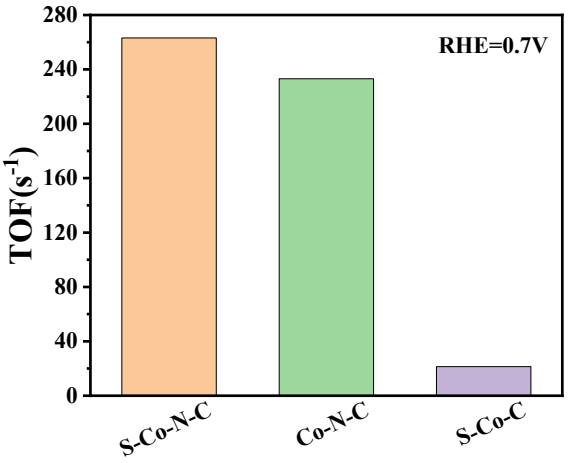

Fig. S34. Estimated TOF values for Co–N–C, S–Co–C, and S–Co–N–C catalysts

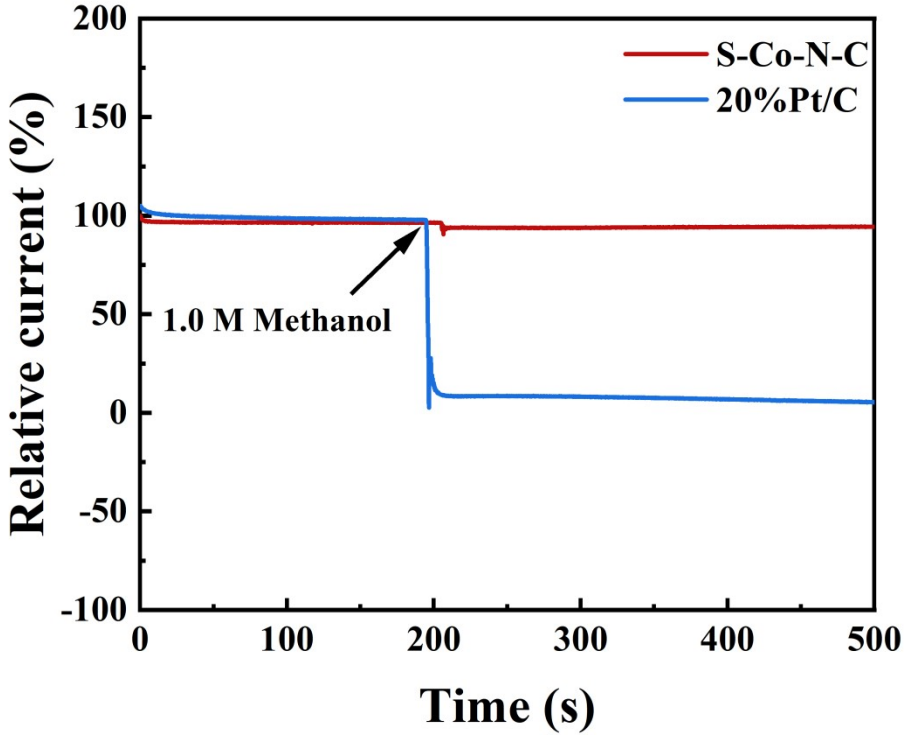

Fig. S35 Methanol poison (i-t) test for S−Co−N−C and Pt/C samples.

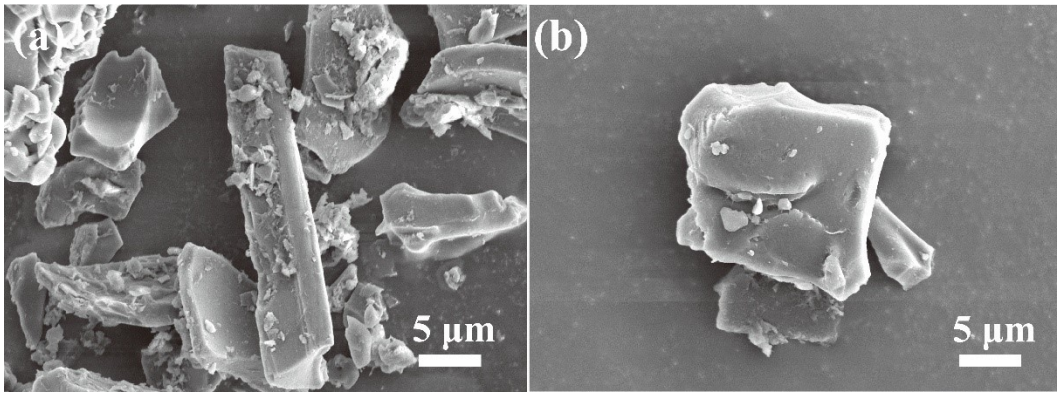

Fig. S36 SEM images after long-term cycling test of S−Co−N−C catalyst

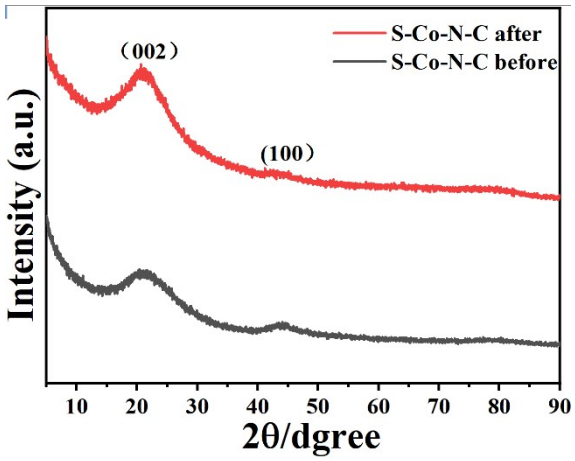

Fig. S37 XRD images before and after long-term cycling test of S−Co−N−C catalyst

Table. S2 Comparison of ORR activity of prepared samples

Catalyst	Limiting diffusion current density(J_L) /mA cm^{-2}	Half-wave potential ($E_{1/2}$) /V *vs.* RHE	onset potential (E_{oneset}) /V *vs.* RHE	Tafel slope /mV dec^{-1}
C	2.71	0.61	0.78	145
NC	3.39	0.69	0.837	162
Co−C	2.70	0.73	0.80	125.4
Co−N−C	3.10	0.78	0.86	72.21
S−N−C	3.04	0.748	0.867	76.25
S−Co−N−C-800	2.40	0.67	0,79	131.7
S−Co−N−C-900	2.88	0.74	0.83	117
S(1)−Co−N−C	3.87	0.75	0.84	93.39
S(2)−Co−N−C	3.27	0.74	0.83	88.16
S−Co−N−C	4.01	0.79	0.89	72.53
20% Pt/C	3.97	0.78	0.93	112.8

Table. S3 Comparison of ORR activity of prepared S−Co−N−C sample with previous reports

Catalyst	Half-wave potential ($E_{1/2}$) /V	Initial potential (E_{onset}) /V	Tafel slope (mV dec^{-1})	Scan rate (V s^{-1})	Electrolyte	References
S−Co−N−C	0.79	0.89	72.53	0.01	0.1 M KOH	**Present study**
CoS_2/N，SGO	0.79	0.97	75	0.01	0.1 M KOH	[13]
$CoSe_2$/N−C	0.71	0.79	-	0.01	0.1 M KOH	[14]
CoNC	0.785	0.89	-	0.01	0.1 M KOH	[15]
Co−N−CNFs	0.7	0.82	-	0.01	0.1 M KOH	[16]
FeN_3P	0.75	0.89	-	0.01	0.1 M KOH	[17]
NiO/CoN PINWs	0.68	0.89	86	0.005	0.1 M KOH	[18]
$NiCo_2O_4$ NWs	0.65	0.86	138	0.01	0.1 M KOH	[18]
Co/CeO_2−NCNA@CC	0.77	-	98	0.01	0.1 M KOH	[19]
BN/Cu/CNT	0.78	0.96	92	0.01	0.1 M KOH	[20]

Table. S4. Comparison of S−Co−N−C based ZAB performance with previous reports

Catalyst	Open circuit potential (V)	Power density (mW cm^{-2})	Specific capacity (mAh·g_{Zn}^{-1})	Electrolyte	References
S−Co−N−C	1.45	135	794	6 M KOH with 0.2 M $Zn(CH_3COO)_2·2H_2O$	**Present study**
Co/Co−N−C	1.434	122.5	700.6	6 M KOH with 0.2 M $Zn(CH_3COO)_2·2H_2O$	21
D−Co@NC	1.41	115.4	745.5	6 M KOH with 0.2 M $Zn(CH_3COO)_2·2H_2O$	22
Co_2P/CoNPC	1.425	116	NA	6 M KOH with 0.2 M $Zn(CH_3COO)_2·2H_2O$	23
Co@SNHC	1.48	105	708.0	6 M KOH with 0.2 M $Zn(CH_3COO)_2·2H_2O$	24
Co, Fe−HNC-1	1.524	85	759.5	6 M KOH with 0.2 M $Zn(CH_3COO)_2·2H_2O$	25
Co@NC@NCNT-750–10	1.427	136.4	722.9	6 M KOH with 0.2 M $Zn(CH_3COO)_2·2H_2O$	26
CoCu/N−CNS	1.45	104.3	879.3	6 M KOH with 0.2 M $Zn(CH_3COO)_2·2H_2O$	27
CoFe−SNC	1.45	76.5	636.3	6 M KOH with 0.2 M $Zn(CH_3COO)_2·2H_2O$	28
Co_2P/Co−N−C	1.55	94	698	6 M KOH with 0.2 M $Zn(CH_3COO)_2·2H_2O$	29

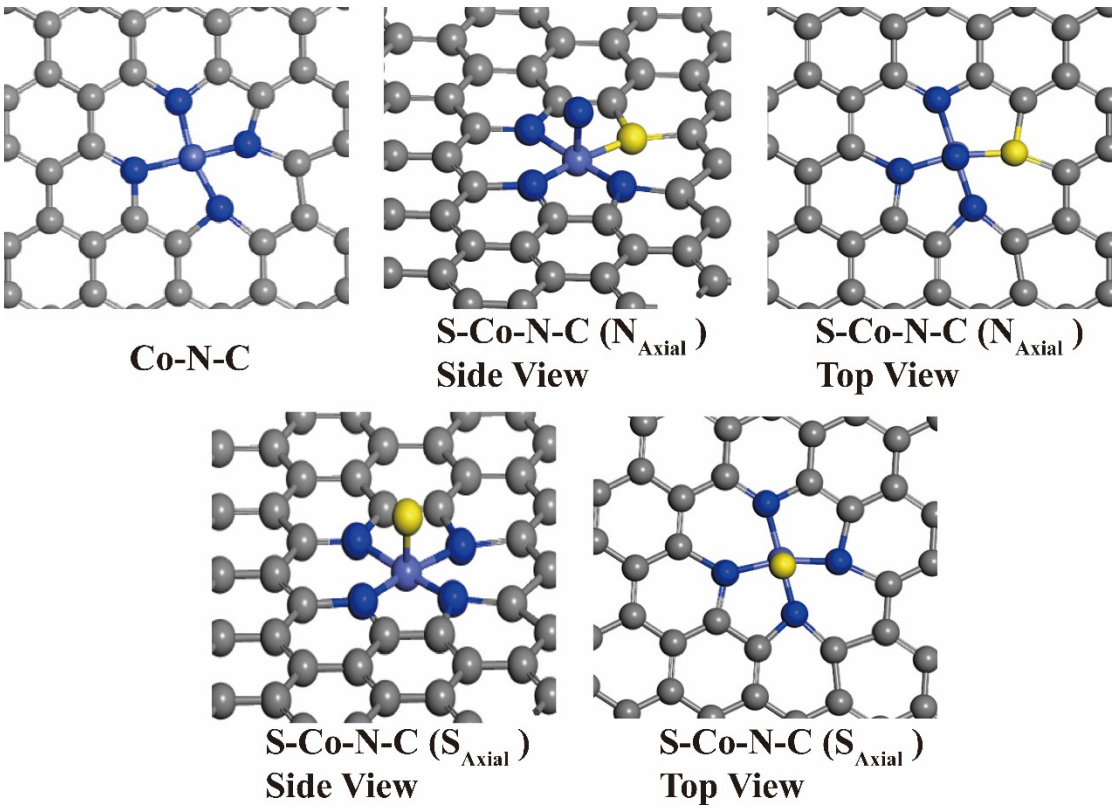

Fig. S38 Optimized atomic structure models comprise single atomic systems Co−N−C, with and without S, isolated SACs systems with S and N at two different configurations.

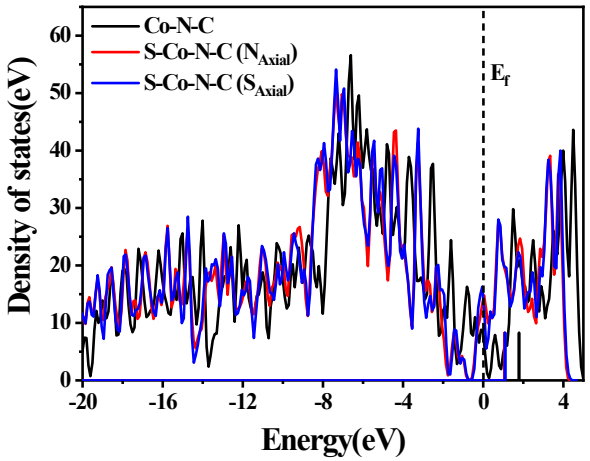

Fig. S39 Total density of states of (TDOS) of S−Co−N−C (N_{Axial}), S−Co−N−C (S_{Axial}) and Co−N−C

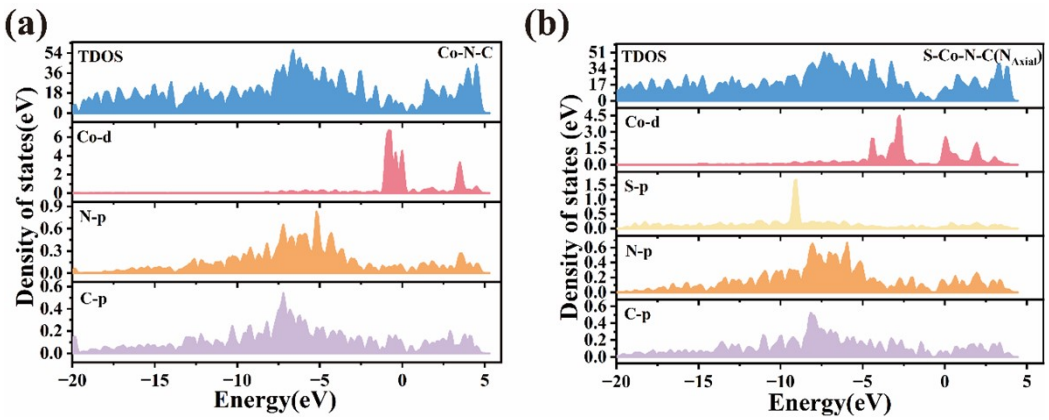

Fig. S40 Partial density of states of (PDOS) of Co−N−C and S−Co−N−C.

References

1. B. Ravel and M. Newville, *Synchrotron Radiation*, 2005, **12**, 537-541.
2. S. Chandrasekaran, R. Hu, L. Yao, L. Sui, Y. Liu, A. Abdelkader, Y. Li, X. Ren and L. Deng, *Nano-Micro Letters*, 2023, **15**.
3. J. Huang, T. Ma, K. Guo, Z. Meng, J. Li, D. Fan, H. Lu, Y. Liu and S. Chandrasekaran, *Composites Part B: Engineering*, 2026, **314**, 113467.
4. X. Yan, D. Liu, P. Guo, Y. He, X. Wang, Z. Li, H. Pan, D. Sun, F. Fang and R. Wu, *Advanced Materials*, 2023, **35**, 2210975.
5. G. Yang, J. Zhu, P. Yuan, Y. Hu, G. Qu, B.-A. Lu, X. Xue, H. Yin, W. Cheng, J. Cheng, W. Xu, J. Li, J. Hu, S. Mu and J.-N. Zhang, *Nature Communications*, 2021, **12**, 1734.
6. C. Di Paola, E. Plekhanov, M. Krompiec, C. Kumar, E. Marsili, F. Du, D. Weber, J. S. Krauser, E. Shishenina and D. Muñoz Ramo, *npj Computational Materials*, 2024, **10**, 285.
7. P. Giannozzi, S. Baroni, N. Bonini, M. Calandra, R. Car, C. Cavazzoni, D. Ceresoli, G. L. Chiarotti, M. Cococcioni, I. Dabo, A. Dal Corso, S. de Gironcoli, S. Fabris, G. Fratesi, R. Gebauer, U. Gerstmann, C. Gougoussis, A. Kokalj, M. Lazzeri, L. Martin-Samos, N. Marzari, F. Mauri, R. Mazzarello, S. Paolini, A. Pasquarello, L. Paulatto, C. Sbraccia, S. Scandolo, G. Sclauzero, A. P. Seitsonen, A. Smogunov, P. Umari and R. M. Wentzcovitch, *Journal of Physics: Condensed Matter*, 2009, **21**, 395502.
8. P. Giannozzi, O. Andreussi, T. Brumme, O. Bunau, M. Buongiorno Nardelli, M. Calandra, R. Car, C. Cavazzoni, D. Ceresoli, M. Cococcioni, N. Colonna, I. Carnimeo, A. Dal Corso, S. de Gironcoli, P. Delugas, R. A. DiStasio, A. Ferretti, A. Floris, G. Fratesi, G. Fugallo, R. Gebauer, U. Gerstmann, F. Giustino, T. Gorni, J. Jia, M. Kawamura, H. Y. Ko, A. Kokalj, E. Küçükbenli, M. Lazzeri, M. Marsili, N. Marzari, F. Mauri, N. L. Nguyen, H. V. Nguyen, A. Otero-de-la-Roza, L. Paulatto, S. Poncé, D. Rocca, R. Sabatini, B. Santra, M. Schlipf, A. P. Seitsonen, A. Smogunov, I. Timrov, T. Thonhauser, P. Umari, N. Vast, X. Wu and S. Baroni, *Journal of Physics: Condensed Matter*, 2017, **29**, 465901.
9. P. E. Blöchl, *Physical Review B*, 1994, **50**, 17953-17979.
10. S. Grimme, J. Antony, S. Ehrlich and H. Krieg, *The Journal of Chemical Physics*, 2010,

132.
11. H. Adabi, A. Shakouri, N. Ul Hassan, J. R. Varcoe, B. Zulevi, A. Serov, J. R. Regalbuto and W. E. Mustain, *Nature Energy*, 2021, **6**, 834-843.
12. C. Chen, Y. Li, A. Huang, X. Liu, J. Li, Y. Zhang, Z. Chen, Z. Zhuang, Y. Wu, W.-C. Cheong, X. Tan, K. Sun, Z. Xu, D. Liu, Z. Wang, K. Zhou and C. Chen, *Journal of the American Chemical Society*, 2023, **145**, 21273-21283.
13. P. Ganesan, M. Prabu, J. Sanetuntikul and S. Shanmugam, *Acs Catalysis*, 2015, **5**, 3625-3637.
14. Y.-S. Chao, D.-S. Tsai, A.-P. Wu, L.-W. Tseng and Y.-S. Huang, *International Journal of Hydrogen Energy*, 2013, **38**, 5655-5664.
15. L. Chen, X. Liu, L. Zheng, Y. Li, X. Guo, X. Wan, Q. Liu, J. Shang and J. Shui, *Applied Catalysis B-Environmental*, 2019, **256**.
16. Q. Cheng, L. Yang, L. Zou, Z. Zou, C. Chen, Z. Hu and H. Yang, *Acs Catalysis*, 2017, **7**, 6864-6871.
17. K. Yuan, D. Luetzenkirchen-Hecht, L. Li, L. Shuai, Y. Li, R. Cao, M. Qiu, X. Zhuang, M. K. H. Leung, Y. Chen and U. Scherf, *Journal of the American Chemical Society*, 2020, **142**, 2404-2412.
18. J. Yin, Y. Li, F. Lv, Q. Fan, Y.-Q. Zhao, Q. Zhang, W. Wang, F. Cheng, P. Xi and S. Guo, *Acs Nano*, 2017, **11**, 2275-2283.
19. S. Li, H. Zhang, L. Wu, H. Zhao, L. Li, C. Sun and B. An, *Journal of Materials Chemistry A*, 2022, **10**, 9858-9868.
20. J. Yu, Z. Jiang, T. Huang and C. Tang, *International Journal of Hydrogen Energy*, 2023, **48**, 20368-20377.
21. D. Wang, P. Yang, H. Xu, J. Ma, L. Du, G. Zhang, R. Li, Z. Jiang, Y. Li and J. Zhang, *Journal of Power Sources*, 2021, **485**, 229339.
22. F. Zhang, L. Chen, H. Yang, Y. Zhang, Y. Peng, X. Luo, A. Ahmad, N. Ramzan, Y. Xu and Y. Shi, *Chemical Engineering Journal*, 2022, **431**, 133734.
23. H. Liu, J. Guan, S. Yang, Y. Yu, R. Shao, Z. Zhang, M. Dou, F. Wang and Q. Xu, *Advanced Materials*, 2020, **32**, 2003649.
24. J. Liu, L. Xu, Y. Deng, X. Zhu, J. Deng, J. Lian, J. Wu, J. Qian, H. Xu and S. Yuan, *Journal of Materials Chemistry A*, 2019, **7**, 14291-14301.
25. Y. Zhang, T. Zhu, Q. Zhong and H. Qu, *Journal of Alloys and Compounds*, 2023, **958**, 170447.
26. J. Li, G. Lai, L. Li and W. Zhang, *Colloids and Surfaces a-Physicochemical and Engineering Aspects*, 2025, **726**.
27. J. Kuang, Y. Shen, Y. Zhang, J. Yao, J. Du, S. Yang, S. Zhang, Y. Fang and X. Cai, *Small*, 2023, **19**, 2207413.
28. C.-C. Weng, J.-T. Ren, H.-Y. Wang, X.-W. Lv, Y.-J. Song, Y.-S. Wang, L. Chen, W.-W. Tian and Z.-Y. Yuan, *Applied Catalysis B: Environment and Energy*, 2022, **307**, 121190.
29. X. Liu, W. Yan, J. Song, H. Song, W. Chen, Y. Zhang and Y. Chen, *Chemical Engineering Journal*, 2024, **492**.